Supplementary Information (SI) for Environmental Science: Nano.

Supporting information

Vertical transport of polystyrene nanoplastics in natural soils under unsaturated conditions: Influence of particle size and texture

Cynthia Rieckhof[1,2*], Virtudes Martínez-Hernández[2*], Ekkehard Holzbecher[3], Raffaella Meffe[2]

[1] University of Alcalá, Geology, Geography and Environment Science Department, Ctra. Madrid-Barcelona KM 33.600, 28802 Alcalá de Henares, Spain

[2] IMDEA Water Institute, Avda. Punto Com 2, 28805 Alcalá de Henares, Spain

[3] GUtech, PO Box 1816, Athaibah PC 130, Muscat, Sultanate of Oman

*Corresponding author (e-mail address: cynthia.rieckhof@edu.uah.es)

*Corresponding author (e-mail address: virtudes.martinez@imdea.org)

Table S1. Summary of physicochemical properties of PSNPs used in the experiments.

PSNP	Particle size (nm)	Colour	ʎex (nm)	ʎem (nm)	Parking area (Å2 group^{-1})	Surface charge density (µC cm$^{2-1}$)	Density (g cm$^{3-1}$)
120	122±1	Pink	576	596	82	19.5	1.054
500	508±3	Pink	576	596	53	42.1	1.054
1000	1009±5	White	375	427	184	30.2	1.054

Table S2. Physicochemical properties of selected porous material

Soil	Texture	Particle composition			Soil organic matter (%)	Electrical conductivity (μS cm^{-1})	pH	Cation Exchange capacity (cmol kg^{-1})
		Sand (%)	Silt (%)	Clay (%)				
SL	Sandy loam	73	12	15	1.49	196	8.05	9.8
CL	Clay loam	23	38	39	1.14	65	8.17	29.3

Text S1. PSNPs concentration measurement

The absorbance of PSNPs was determined using a UV-1800 UV-VIS spectrophotometer (Shimadzu, Japan) at a specific wavelength (Table S3). Linear calibration curves were used to calculate the concentration of the PSNPs in the influent (tap water) and effluent (matrix water) samples. Calibration curves were performed by spiking PSNPs in the tap water and matrix water to account for soil interferences. Method detection limit (MDL) and method quantification limit (MQL) are presented in Table S3. Values below the MDL are considered as zero for calculations. Standard calibration curves for 120, 500 and 1000 nm PSNP from column experiments are presented in tap water (Figs. S1–S3, left) and in SL (Figs. S1–S3, right), and CL matrix waters (Fig. S4), Calibration curves from batch sorption–desorption experiments in SL matrix waters are shown in Fig. S5. Despite the calibration curves obtained for the 1000 nm PSNPs in the sorption–desorption experiments with soil SL showed coefficients of determination (R^2) greater than 0.99, the samples could not be reliably quantified due to potential interferences from the matrix. In some cases, the measured concentrations exceeded the initial spiked values. In other cases, the characteristic shape of the PSNP spectrum was irregular or absent. This problem was not observed in the batch experiments with 120 nm and 500 nm PSNPs nor in the column infiltration experiments with 1000 nm PSNP, since the column undergoes chemical and hydrodynamic stabilisation, resulting in more stable and reliable effluent samples.

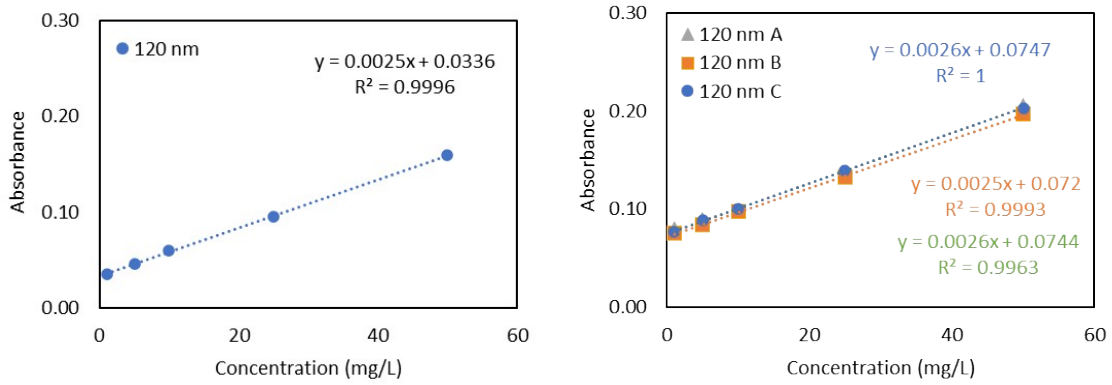

Fig. S1. Standard calibration curve for 120 nm PSNP in tap water (left) and in SL matrix water (right) for each replicate.

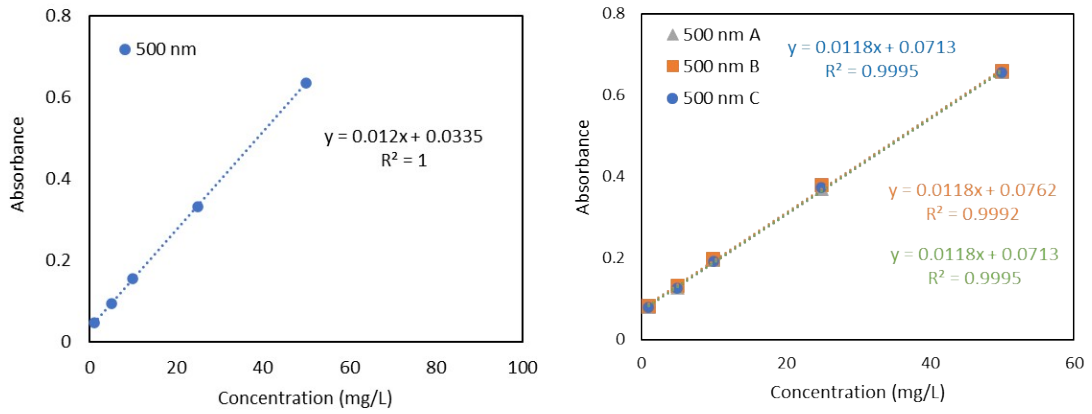

Fig. S2. Standard calibration curve for 500 nm PSNP in tap water (left) and SL matrix water (right) for each replicate.

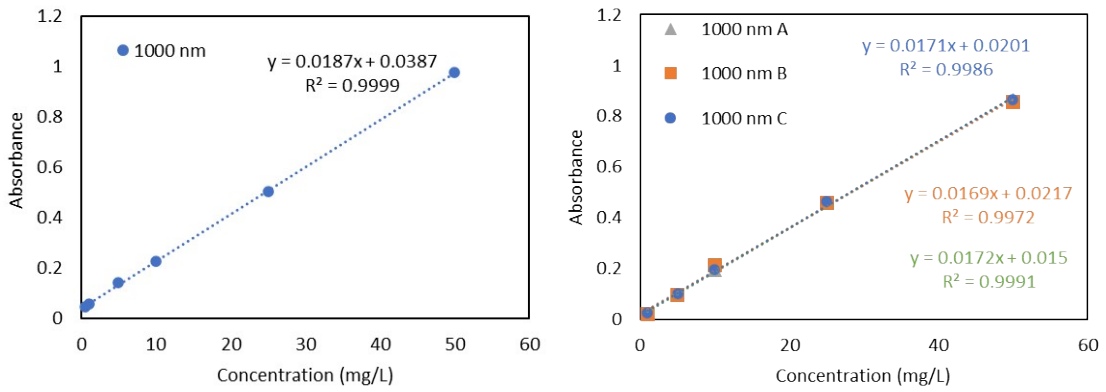

Fig. S3. Standard calibration curve for 1000 nm PSNP in tap water (left) and SL matrix water (right) for each replicate.

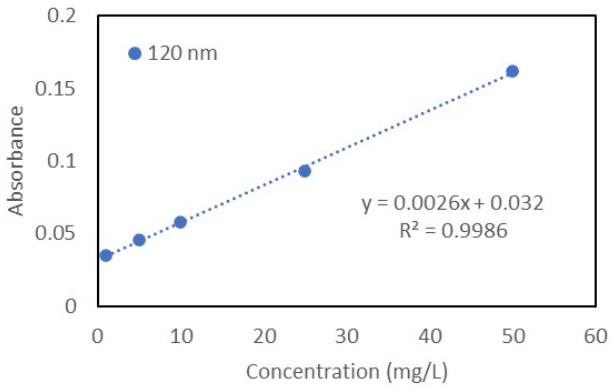

Fig. S4. Standard calibration curve for 120 nm PSNP in CL matrix water (right).

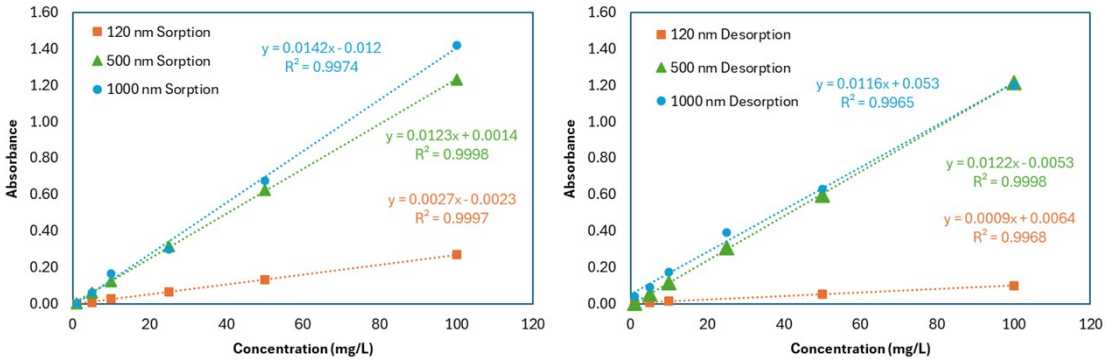

Fig. S5. Standard calibration curves for 120, 500 and 1000 nm PSNP in SL matrix water from batch sorption (right) and desorption (right) experiments.

Table S3. Excitation and emission wavelengths, method detection limit (MDL) and method quantification limit (MQL) of PSNPs

Porous media	PSNP (nm)	ʎex (nm)	ʎem (nm)	MDL (mg L^{-1})	MQL (mg L^{-1})
Soil SL	120	576	596	0.69	2.31
	500	576	596	0.75	2.50
	1000	375	427	0.31	1.06
Soil CL	120	576	596	1.15	3.83

Text S2. XDLVO theory calculations

The total interaction energy (V_{TOT}) between NP-NP, NP-Soil and NP-AWI was calculated applying the extended Derjaguin-Landau-Verwey-Overbeek (DLVO) theory. V_{TOT} (1) is described as the sum of the repulsive electrostatic double layer interaction V_{EDL} (2, 3), the attractive van der Waals interaction V_{VDW} (5, 6) and the Lewis acid-base interaction (7).

$$V_{TOT} = V_{VDW} + V_{EDL} + V_{AB} \quad (1)$$

The repulsive electrostatic double layer interaction (Gregory, 1975) is expressed as (2) for NP-NP interaction and (3) for NP-Soil and NP-AWI interaction.

$$V_{EDL} = 2\pi r_{NP}\varepsilon_0\varepsilon_r\phi_p^2\{2\phi_p \ln[1 + \exp(-kh)\} \quad (2)$$

$$V_{EDL} = \pi r_{NP}\varepsilon_0\varepsilon_r\left\{2\phi_p\phi_c \ln\left[\frac{1 + \exp(-kh)}{1 - \exp(-kh)}\right] + \left(\phi_p^2 + \phi_c^2\right)\ln[1 - \exp(-2kh)\right\} \quad (3)$$

Where r_{NP} is the NP radius (m), $\mathcal{E}_O$ is the vacuum permittivity (8.854 x 10^{-12} C V^{-1} m^{-1}), $\mathcal{E}_r$ is the relative dielectric permittivity of water (78.5), ϕ_p is the zeta potential of NP (-12.2, -18.5 and -31.5 for 120, 500 and 1000 nm PSNPs) and ϕ_c is the zeta potential of the soil (2.41 mV) and AWI [-46.5 mV (Dong et al., 2022)]; and k is the Debye-Hückel parameter, defined by (4)

$$k = \sqrt{\frac{2N_A e^2 I}{\varepsilon_0\varepsilon_r K_B T}} \quad (4)$$

where N_A is Avogadro's number ($6.02 \cdot 10^{23}$ mol^{-1}), e is the electron charge (-1.60 x 10^{-19} C), I is the ionic strength of the background electrolyte solution (1.3E-02 mol l^{-1}), K_B is Boltzmann constant (1.38 x 10^{-23} J K^{-1}), and T is temperature (298 K).

The attractive van der Waals interaction (Gregory, 1981) is expressed as (5) for NP-NP interaction and (6) for NP-Soil and NP-AWI interaction.

$$V_{VDW} = -\frac{A_{131}\, r_{NP}}{6h\left(1 + \frac{14h}{\lambda}\right)} \quad (5)$$

$$V_{VDW} = -\frac{A_{132}\, r_{NP}}{6h\left(1 + \frac{14h}{\lambda}\right)} \quad (6)$$

where A_{131} represents the Hamaker constant for NP-NP [-4,2 x 10^{-21} J (Israelachvili, 1992)], A_{132} represents the Hamaker constant for NP-Water-Soil and NP-Water-Air [4.04 x 10^{-20} J ((Wu et al., 2020) and -1.2 x 10^{-20} J (Israelachvili, 1992), respectively], h is the separation distance between NP and soil surface or AWI (m) and λ is the characteristic wavelength of interaction (10^{-7} m) (Elimelech et al., 1995).

The Lewis acid-base interaction (Van Oss, 1993) is expressed as (7) for NP-Soil interaction.

$$V_{AB} = 2\pi r\lambda_w \Delta G_{h_0}^{AB} exp^{(\frac{h_0 - h}{\lambda_w})} \quad (7)$$

where λ_w is the characteristic decay length (0.6 nm) of acid-base interactions in water, h_0 is the minimum equilibrium distance (0.157 nm) between NPs and soil surface and $\Delta G_{h_0}^{AB}$ is calculated as (8):

$$\Delta G_{h_0}^{AB} = 2\left[\sqrt{\gamma_w^+}\left(\sqrt{\gamma_{NP}^-} + \sqrt{\gamma_s^-} - \sqrt{\gamma_w^-}\right) + \sqrt{\gamma_w^-}\left(\sqrt{\gamma_{NP}^+} + \sqrt{\gamma_s^+} - \sqrt{\gamma_w^+}\right) - \sqrt{\gamma_{NP}^-\gamma_s^+} - \sqrt{\gamma_{NP}^+\gamma_s^-}\right]$$

where the subscripts *NP*, *w* and *s* represent NPs, water and soil, respectively. Υ^+ and Υ^- represent the electronics accepting and donating interfacial tensions, which values are $\gamma_w^+ = \gamma_w^- = 25.5$ mJ/m^2, $\gamma_s^+ = 1.4$ mJ/m^2, $\gamma_s^- = 47.8$ mJ/m^2, $\gamma_m^+ = 0.02$ mJ/m^2, and $\gamma_m^- = 7.6$ mJ/m^2 (Gallardo et al., 2002: Sun et al., 2015).

Table S4. Model input parameters of the best fit replicate for each experiment.

Parameter		NP	
		120 nm	**500 nm**
Model domain	Profile length (cm)	10	
	No. of materials	1	
	No. of nodes	101	
Time domain	Output time step (min)	6.67	
	Simulation time (min)	667	
Hydraulic properties	Bulk density (g cm^{-3})	1.51	
	Flux (mL min^{-1})	0.52	0.53
	Porosity (-)	0.39	0.37
	Saturation (%)	77.6	83.4
Initial conditions	KCl (g L^{-1})	0	
	NP (mg L^{-1})	0	
Boundary conditions	Dirichlet at inlet		
	Neumann at outlet		
Parameter estimation methods	Levenberg-Marquardt		
	SNOPT		
	BOBYA		

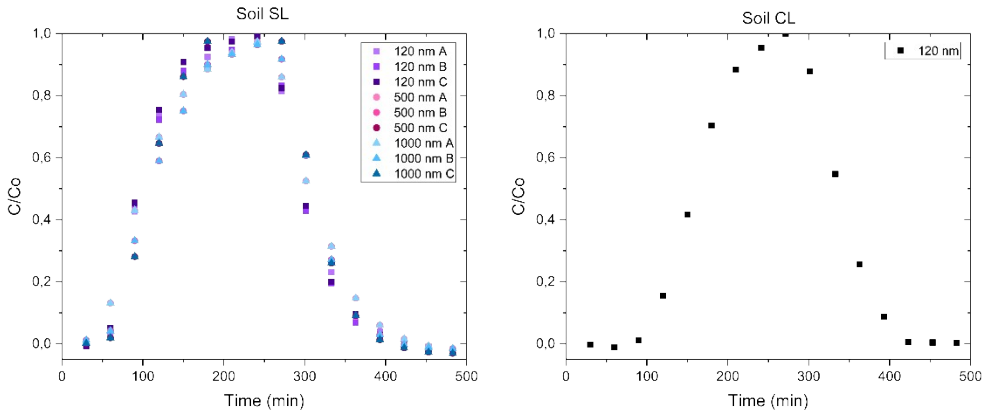

Fig. S6. Experimental breakthrough curves of the tracers (KCl) obtained during infiltration using soils SL (left) and CL (right).

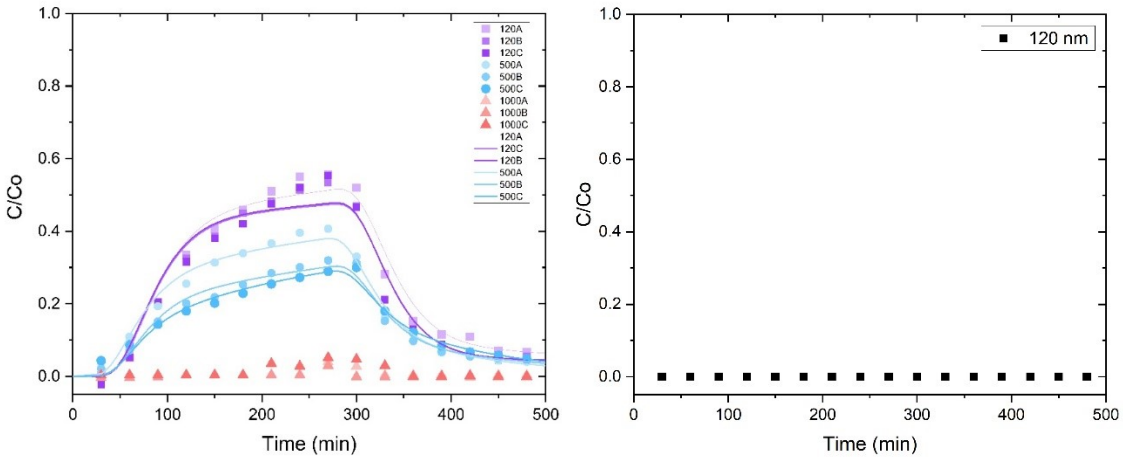

Fig. S7. Experimental (in dots) and simulated (in solid lines) breakthrough curves from the replicates of infiltration column experiments with 120, 500 and 1000 nm PSNPs in Soil SL (left) and CL (right).

References

Dong, S., Zhou, M., Su, X., Xia, J., Wang, L., Wu, H., Suakollie, E.B., Wang, D., 2022. Transport and retention patterns of fragmental microplastics in saturated and unsaturated porous media: A real-time pore-scale visualization. *Water Res 214*. https://doi.org/10.1016/j.watres.2022.118195

Elimelech, M., Gregory, J., Jia, X., Williams, R.A., 1995. *Particle Deposition & Aggregation*. Elsevier. https://doi.org/10.1016/B978-0-7506-7024-1.X5000-6

Gallardo-Moreno, A. M.; Gonzalez-Martin, M. L.; Perez-Giraldo, C.; Garduno, E.; Bruque, J. M.; Gomez-Garcia, A. C., 2002. Thermodynamic Analysis of Growth Temperature Dependence in the Adhesion of Candida parapsilosis to Polystyrene. *Appl. Environ. Microb. 68, (5),* 2610-2613.

Gregory, J., 1981. Approximate expressions for retarded van der waals interaction. *J Colloid Interface Sci 83,* 138–145. https://doi.org/10.1016/0021-9797(81)90018-7

Gregory, J., 1975. Interaction of unequal double layers at constant charge. *J Colloid Interface Sci 51,* 44–51. https://doi.org/10.1016/0021-9797(75)90081-8

Israelachvili, J., 1992. Interfacial forces. *Journal of Vacuum Science & Technology A: Vacuum, Surfaces, and Films, 10(5),* 2961-2971. https://doi.org/10.1116/1.577894

Sun, Y.; Gao, B.; Bradford, S. A.; Wu, L.; Chen, H.; Shi, X.; Wu, J., 2015. Transport, retention, and size perturbation of graphene oxide in saturated porous media: effects of input concentration and grain size. *Water Res.68*, 24-33

Van Oss, C. J. (1993). Acid—base interfacial interactions in aqueous media. *Colloids and Surfaces A: Physicochemical and Engineering Aspects*, *78*, 1-49.

Wu, X., Lyu, X., Li, Z., Gao, B., Zeng, X., Wu, J., Sun, Y., 2020. Transport of polystyrene nanoplastics in natural soils: Effect of soil properties, ionic strength and cation type. *Sci Total Environ. 707*. https://doi.org/10.1016/j.scitotenv.2019.136065